Delft University of Technology

Monitoring bolt tightness of rail joints using axle box acceleration measurements

Oregui, M; Li, S.; Nunez, Alfredo; Li, Z; Carroll, R; Dollevoet, RPBJ

Citation (APA)
Oregui, M., Li, S., Nunez, A., Li, Z., Carroll, R., & Dollevoet, RPBJ. (2016). Monitoring bolt tightness of rail joints using axle box acceleration measurements. *Structural Control and Health Monitoring: the bulletin of ACS*, *24*(2). https://doi.org/10.1002/stc.1848

Important note
To cite this publication, please use the final published version (if applicable).
Please check the document version above.

Monitoring bolt tightness of rail joints using Axle Box Acceleration Measurements

M. Oregui[1], S. Li[1], A. Núñez[1], Z. Li[1*], R. Carroll[2] and R. Dollevoet[1]

[1]*Delft University of Technology, Faculty of Civil Engineering and Geosciences, Section of Railway Engineering, Stevinweg 1, 2628 CN Delft, the Netherlands*

[2]*Stagecoach Supertram Maintenance Ltd, Nunnery Depot, Woodbourn Road, Sheffield, S9 3LS, United Kingdom*

SUMMARY

Rail joints are a weak component in railway tracks because of the large impact and wheel-rail contact forces. Every train passage contributes to the deterioration of rail joints, causing visible (e.g. battered rails) and invisible (e.g. loose bolts) damages. The invisible damage cannot be detected by the commonly performed visual inspection, which is labor intensive, unreliable, intrusive and unsafe. In this paper, a vehicle-borne monitoring system is used to automatically detect and assess the tightness condition of bolts at rail joints. The monitoring method is developed based on field Axle Box Acceleration (ABA) measurements using different bolt tightness conditions. The suitability of the method is assessed by bolt tightness prediction and verification of a set of rail joints in the tram network of Sheffield, United Kingdom. The results show that ABA system can be employed to monitor bolt tightness conditions at rail joints. With this information better planning for selective preventive maintenance actions can be taken over rail joints. Copyright © 2014 John Wiley & Sons, Ltd.

1. INTRODUCTION

Rail joints (RJs) are an important component in many railway networks worldwide; an example of a RJ is shown in Figure 1a. Although the use of continuously welded rail is nowadays more cost

*Correspondence to: Delft University of Technology, Faculty of Civil Engineering and Geosciences, Section of Railway Engineering Stevinweg 1, 2628 CN Delft, the Netherlands. E-mail: z.li@tudelft.nl

effective due to its significantly longer service life (1), many rails are still connected by rail joints. Furthermore, insulated rail joints (IRJs), in which the two rail ends are separated with an insulating material, are a fundamental component of the safety system in many railway networks.

Figure 1. Two examples of rail joints: (a) invisible damage: loose bolts, and (b) visible damage: missing bolt and battered rail surface

When wheels roll over the discontinuity between rail ends, large impact and dynamic wheel-rail contact forces occur accelerating the deterioration of RJs (2; 3; 4; 5; 6). Bolts get loose, rail joints ends become battered, and cracks develop in the rail. These damage conditions at severe state may lead to rail break, derailment and malfunctioning of the signaling system. In addition, impact noise is a nuisance for the people living nearby railway tracks. To guarantee safety and acceptable noise levels, cost-expensive maintenance measures are taken, usually at a late stage when the only solution is replacement of RJs.

The inspection of RJs is mostly performed visually, which is subjective and labor expensive, and often intrusive and unsafe, such as in 24/7 tram and metro networks. Furthermore, there is the additional challenge of assessing the real damage state of RJs. For instance, the RJ shown in Figure 1b can be easily assessed: one bolt is missing and the rail ends are plastically deformed. Thus, this RJ can be tagged as "severely damaged". However, the condition of the RJ shown in Figure 1a is visually unknown. Although the RJ seems to be in good condition to the naked eye, cracks in the rail web could be present or the bolts could be loose.

To overcome the limitations of visual inspection and improve safety conditions, vehicle-born monitoring systems have been developed in recent years (see a review in (7)). High quality videos and photos are taken from inspection vehicles, but the detection range of this system is limited to visible damage, such as missing fastenings (8). Vehicle-borne ultrasonic measurements are also an alternative, used to detect surface and internal rail defects (9; 10), but its reliability is also limited (11). Different types of deterioration, such as loose bolts or plastic deformation, cannot be detected with ultrasonic measurements.

A vehicle-borne monitoring system that may be able to detect different types of visible and invisible damage at RJs is the Axle Box Acceleration (ABA) system (12; 13; 14; 15; 16). The damage detection method used by the ABA system is based on changes in the dynamic behavior of vehicle-wheel/rail-track interaction. The response of a track is defined by its components and their interaction, so that if one component deteriorates, the track response changes in the signature tunes of the damage condition (i.e. characteristic frequencies and amplitudes). In the case of a RJ, vehicle-track dynamics are excited when the wheel impacts the rail at the discontinuity and the dynamic behavior of RJs changes for different visible damage states (17). In view of these promising results, we are encouraged to study if ABA systems can detect invisible deterioration.

In this paper, we assess the capacity of an ABA system for evaluating bolt tightness condition at RJs. For this purpose, a field test was carried out in which a vehicle with an ABA system run over a reference RJ with different bolt tightness conditions for calibration, and then over a set of other RJs for trial detection and verification. The paper is organized as follows. In Section 2, the measurement devices are described. In Section 3, a method for detecting bolt tightness condition based on wavelet analysis is introduced. In addition, a designed test performed with resilient wheels at a reference RJ under controlled conditions is shown. In this manner, a theoretical set of values is obtained to make a comparison and assessment of the effectiveness of the methodology. In Section 4, a case study in Sheffield is presented to evaluate the detection method for two RJs. The results are discussed in Section 5 and the main conclusions are summarized in Section 6.

2. RAILWAY TRACK MEASUREMENTS

To assess the feasibility to automatically detect bolt tightness variation at rail joints, two measurements types were performed: axle box accelerations and rail vertical-longitudinal profile. For the former, the ABA system used is presented in Section 2.1 and for the later, the Railprof measurement system is presented in Section 2.2.

2.1. ABA system

ABA systems are dynamic-response-based vehicle-borne measurements (13; 14; 15; 12; 16). As it is schematically shown in Figure 2, the ABA system consists of three main components. First, accelerometers are mounted on axle boxes to measure acceleration. Second, the position of the vehicle is received in a GPS antenna. Third, the vehicle speed is usually obtained from a tacometer.

The measured accelerations contain information of the wheel-track structure. When the track has deteriorated, changes with respect to healthy tracks measurements appear in the measured signals, which are called signature tunes. By detecting signature tunes in the response, deteriorated locations can be traced back by combining the measured position and vehicle speed. However, each track defect type has its own signature tunes, which needs to be determined in advance by defining the characteristic frequencies of interest. Thus, track defects can be detected only if their characteristic frequencies are known. After detection, deterioration state of defects can be assessed so that corrective maintenance measures can be planned according to the damage severity. For example, an ABA system can successfully be used to automatically detect both severe and early stage squats, which are a short wave defect on the rail top (18).
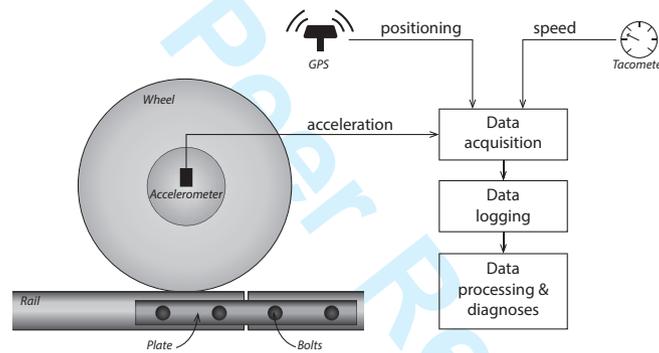

Figure 2. Schematic view of the ABA measuring and diagnosis system

In this paper, the ABA system was mounted on a regular Supertram tram with resilient wheels in Sheffield (see Figure 3). Four accelerometers were mounted on the four axle boxes of a bogie to register acceleration measurement. The lower close-up in Figure 2 shows a sensor mounted on the Supertram bogie. The accelerometers are of piezoelectric type (MEMS), and have a range of ±100g, a frequency bandwidth of 30 kHz, and a sensitivity of 50 mV/g. The accelerometer chosen is suitable for railway application as a similar instrumentation has been under extensive test in The Netherlands for mainline applications (15).

The upper close-up in Figure 3 shows the location of the positioning GPS antenna on the tram roof. The speed signal was obtained from the meter cabinet of the tram. The accelerations, speed and position were recorded in a data acquisition system on-board of the Supertram test tram.

Figure 3. ABA system used with close-ups of the GPS antenna and an accelerometer

2.2. Rail vertical geometry

Rail vertical-longitudinal profiles were measured using the Railprof measurement device (19), see Figure 4a. This measurement is used to better understand the condition of the RJs, specifically with respect to the status of the alignment of the rail ends.

Measurements of the rail profile at rail joints were taken every 5 mm along a length of 1000 mm. The accuracy is ± 0.03 mm, if the deviation between the first and last measuring point in a straight line is less than 0.5 mm. An example of rail vertical-longitudinal profile at a rail joint is shown in Figure 4b The sharp deep indicates the location of the gap. In this case, the two rail ends are misaligned by 0.5 mm, whereas the amplitude of the rest of the waves observed is substantially smaller, i.e. approximately 0.1 mm. Thus, the misalignment is expected to influence the wheel-track response more significantly than the rest of the measured waves. Furthermore, from unloaded to loaded conditions, the dip of the rail joint could increases three times (2; 20). Thus, the discontinuity is significantly more prominent when the train is rolling over the rail joint than during the measurements with the Railprof.

3. EVALUATION METHOD FOR BOLT TIGHTNESS CONDITION BASED ON WAVELETS

To develop the detection method for bolt tightness condition at RJs, a controlled field test with different measurable bolt tightness levels is proposed at a reference RJ. Thus, by analyzing the frequency components under the different conditions, signature tunes and detection algorithms for bolt tightness can be developed. The number of reference RJ and the tightness condition applied depends on the accuracy required. At least three different conditions are recommended (loose, half-tight and tight) so that a clear trend of the signature tunes can be obtained. For the case study in
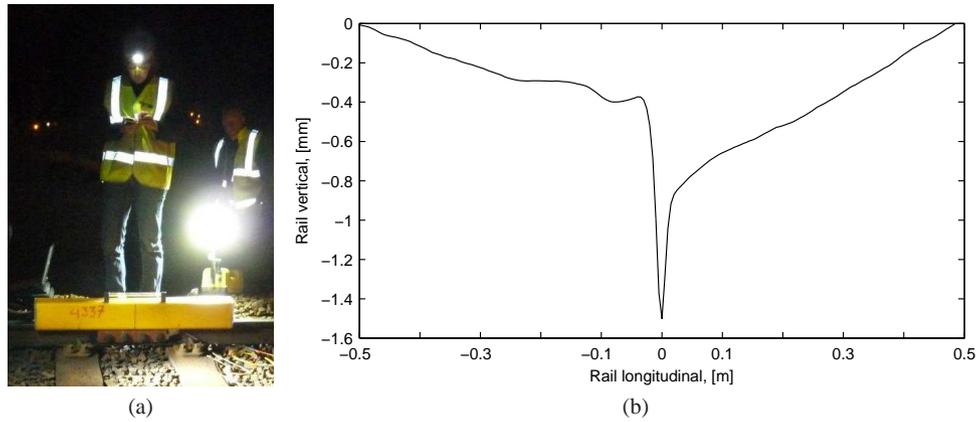
(a)   (b)

Figure 4. Rail vertical-longitudinal profile measurement: (a) field measurement and (b) a measured profile

this paper, five tightness conditions were considered at the reference RJ. Each of the five torque conditions were applied equally to all the four bolts except for one case as indicated in Figure 5. The five tightness condition cases are:

- 320 Nm

- 270 Nm (nominal torque)

- 150 Nm

- 150 Nm - 0 Nm (see Figure 5)

- 0 Nm

For each bolt tightness case, multiple measurements of acceleration were taken at the axle boxes by running the vehicle over the reference RJ with a speed of 21km/h. As the track studied was bidirectional, measurements in both directions A (i.e. Depot-Meadowhall) and B (i.e. Meadowhall-Depot) were obtained and analyzed separately. To analyze the alignment between rail ends, rail vertical-longitudinal profile at the reference RJ was also measured.
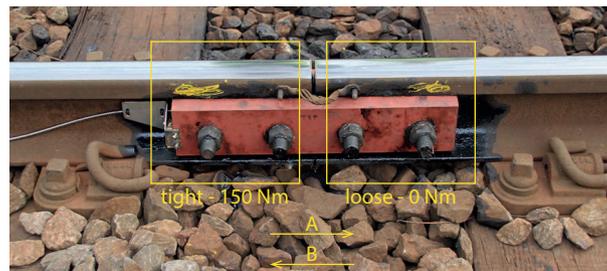

Figure 5. Reference rail joint. The non-uniform 150 Nm - 0 Nm tightness condition and the A and B traffic directions are shown.

3.1. ABA measurements in the time domain

Figure 6a shows the resulting vibrations at the axle of the vehicle-track interactions in the proximity of the reference RJ. Thus, many vibrations are included in the final measured signal. To extract the information related to rail joint bolt tightness condition, the signals were band-pass filtered between 150 and 1200 Hz (see Figure 6b). This was necessary to remove the frequency components lower than 150 Hz which had a high energy concentration due to the low vehicle speed (21 km/h) and which would otherwise have submerged the frequency components related to the bolt tightness condition of the RJs at this speed. At frequencies higher than 1200 Hz, no relevant energy concentrations were observed.
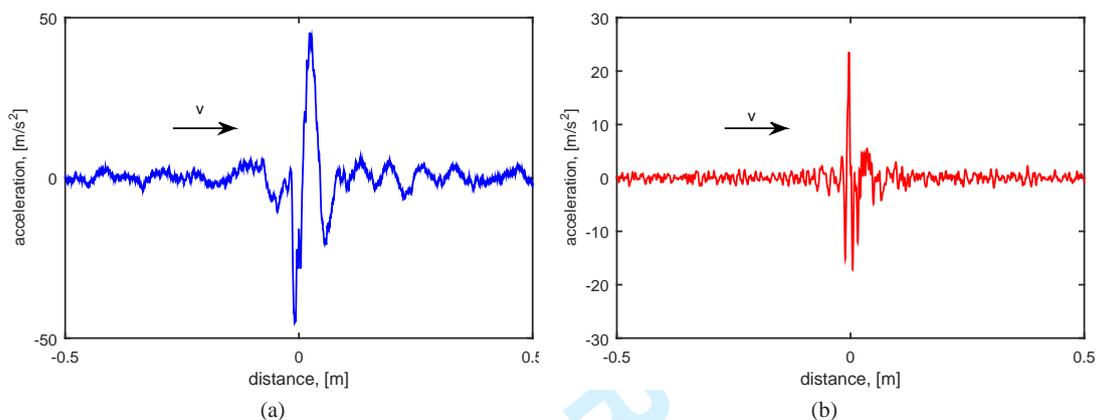

Figure 6. Example of measured ABA accelerations at a RJ: (a) without filter and (b) with a band-pass filter of 150-1200 Hz.

3.2. Data analysis based on wavelets

The wavelet transform analysis is used to extract signature tunes from the ABA measurements. With wavelet transform, the energy content of the accelerations can be obtained as a function of frequency and position along the track. One major advantage of wavelets is that the time-frequency representation is not dependent on the scale (or window size). Therefore, wavelet analysis is appropriate for investigation of non-stationary phenomena with local changes in the frequency components. For example, the frequency range and position of track irregularities, such as rail joints, can be identified.

Continuous wavelet transform (CWT) is a time-frequency analysis tool, where convolutions of the analyzed signal with a group of shifted and scaled wavelet functions are calculated (21). CWT

can be defined according to (1).

$$W_x\left(s,\tau\right) = \int_{-\infty}^{\infty} x(t)\frac{1}{\sqrt{s}}\psi^*\left(\frac{t-\tau}{s}\right)dt \tag{1}$$

where $x(t)$ is the analyzed signal, $\psi(t)$ is a mother wavelet, $\frac{1}{\sqrt{s}}\psi\left(\frac{t-\tau}{s}\right)$ is a family of wavelets deduced from the mother wavelet by different translations and scaling, τ is a continuous variable for the translations, s is a wavelet scale with $s > 0$, and $*$ indicates a complex conjugate. In this work, the Morlet function (2) is used as mother wavelet.

$$\psi_0\left(\eta\right) = \pi^{-1/4}e^{i\omega_o\eta}e^{-\eta^2/2} \tag{2}$$

where ω_0 is a non-dimensional frequency.

To analyze the most relevant frequency components in a signal, the wavelet power spectrum diagram (or scalogram) is calculated using the square of the wavelet coefficients $\left|W_x^2\left(s,\tau\right)\right|$. An example of ABA acceleration and its scalogram for measurements over a rail joint is shown in Figure 7. The rolling distance is shown on the horizontal axis, whereas frequency is indicated on the vertical axis. In this case, a measurement along 1 meter is shown with the discontinuity of the RJ at 0 mm. The frequencies shown are between 150 and 1200 Hz. The amount of energy concentrated at a certain frequency and location is indicated with different colors according to the colorbar. Blue means low energy concentration, whereas red means high energy concentration.
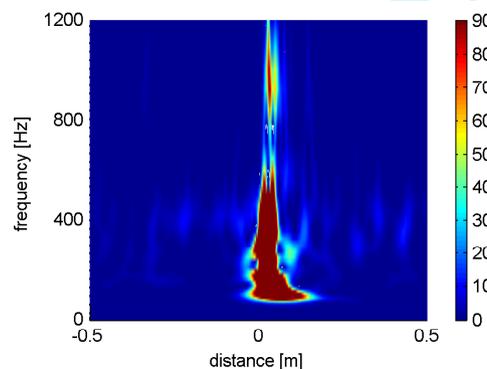

Figure 7. Example of scalogram from ABA measurements at a RJ.

In this example, there is a high energy concentration between 150 and 400 Hz along 0.1 m after the discontinuity. This frequency range results to be the signature tune for bolt tightness analysis, which will be deducted in Section 3. In addition there is a high frequency component at approximately

1000 Hz just after the discontinuity. Due to its short duration and the high frequency, it is most likely closely related to the wheel-rail impact. These frequency ranges are investigated in Section 3.

The wavelet diagrams give a good overview of the energy distribution in frequency and location. However, similarities and differences in frequency between measurements are difficult to quantify. To facilitate the comparison, global wavelet spectra $\overline{W}^2(s, \tau)$ are computed, which are defined as the wavelet spectrum averaged over the spectra (22). The global wavelet spectrum is calculated in a discretized procedure, according to (3). The values of $\overline{W}^2(s, \tau)$ estimates the power spectrum of a time series in an unbiased and consistent manner (23).

$$\overline{W}^2(s, \tau) = \frac{1}{N} \sum_{n=0}^{N-1} |W_n(s, \tau)|^2 \tag{3}$$

where N is the number of position points. The magnitude of the impact between wheel and rail fluctuates for different bolt tightness conditions, so that the global wavelet spectrum reaches different energy values. To facilitate the comparison between different cases, global wavelet spectra are normalized by its maximum value, see (4).

$$\overline{W}_{\mathrm{N}}^2(s, \tau) = \frac{\overline{W}^2(s, \tau)}{\max_{s,\tau}\left\{\overline{W}^2(s, \tau)\right\}} \tag{4}$$

3.3. Reference rail joint analysis

Figure 8 shows the scalograms of the measured accelerations when the tram was running in the B direction for the five tightness conditions proposed in the methodology. Two tram passages are shown for each bolt loading conditions. The two measurements do not show exactly the same frequency distribution and energy magnitude. This slight disagreement is because the wheels may not run precisely along the same trajectory over the rail so that the wheel-rail contact and the stiffness of the system differ to certain degree each time. This means that each measurement collects the general characteristics of the system, in this case, for instance, the energy concentration between 150 and 600 Hz, as well as local characteristics which depend on the contact location. Figure 8b corresponds to the wavelet power spectrum diagram of the nominal bolt tightness condition (i.e. 270 Nm). For the nominal condition, most of the energy is concentrated between the beginning of the gap at 0 m and the 3rd bolt at 0.05 m. The dominant frequency range covers between 150 and 600 Hz. Moreover, the measurement shows energy concentration at approximately 920 Hz immediately after the gap. No energy concentration is noticed at the end of the RJ at 0.20 m.

10   M. OREGUI ET AL.

To facilitate the comparison of the responses at different bolt tightness conditions, the global wavelet spectra were calculated and the obtained values were normalized by their corresponding maximum value, as explained in the previous section. Figure 8 shows the normalized global wavelet spectrum for the A and B traffic directions. First, all the measurements show a dominant peak between 380-420 Hz which can be identified as the characteristic frequency of the reference RJ. This is not the axial tyre mode of the resilient wheel calculated at 433 Hz (see the numerical modal analysis of the resilient wheel in Appendix A) because this mode vibrates in the axial direction whereas the ABA measurements are in the vertical direction. Furthermore, the rubber layer of the wheel performs a decoupling between the tyre and the web so that tyre modes barely disturb the web and axle, on which the sensors were mounted. The maximum energy is concentrated on the 380-420 Hz peak, except when the plate is completely loose (i.e. 0 Nm in Figure 8j). Thus, when the rail joint does not fulfill its purpose of connecting the two rail ends, the dominant frequencies changes with respect to the nominal conditions. Second, different running directions of the tram result in different normalized global wavelet spectrum diagrams. If bolts are looser, energy concentrates at low frequencies. If the tram travels in the A direction, loose bolts mean the appearance of a dominant frequency around 250 Hz. This trend is observed by comparing the 150Nm, 150-0Nm and 0Nm cases in Figures 8h, 8i and 8j, respectively. Whereas if the tram travels in the B direction, loose bolts mean the appearance of one dominant frequency around 150 Hz and another at approximately 920 Hz. As the 250 Hz component is only observed in one direction, this frequency does not correspond to the flexural axle mode of the resilient wheel (see Appendix A) because then, it should be present in the measurements of both directions.

The differences between the two traffic directions were further investigated by analyzing the measured rail vertical-longitudinal profiles. Figure 9 shows that there was a misalignment between the rail ends. The misalignment seems not compatible with the traffic directions because traffic runs in both directions so that symmetric rail end geometry was expected. Rail end misalignment was most probably caused by the field test, in which the reference RJ was reassembled one week before the test, and during the test the tightness of bolts was changed from nominal value to being completely loose. This misalignment is therefore a disturbance to the local track system, and is causing impact between wheel and rail when the tram is traveling in the B direction. This impact explains the difference between the two directions. Due to the impact, a significant amount of energy concentrates at approximately 920 Hz when the wheel rolls from the gap to the end of the rail joint at 0.2 m. This presence of the energy concentration is not observed in the A direction. As it is shown

(a) 320 Nm   (b) 270 Nm   (c) 150 Nm   (d) 150-0 Nm   (e) 0 Nm

(f) 320 Nm   (g) 270 Nm   (h) 150 Nm   (i) 150-0 Nm   (j) 0 Nm
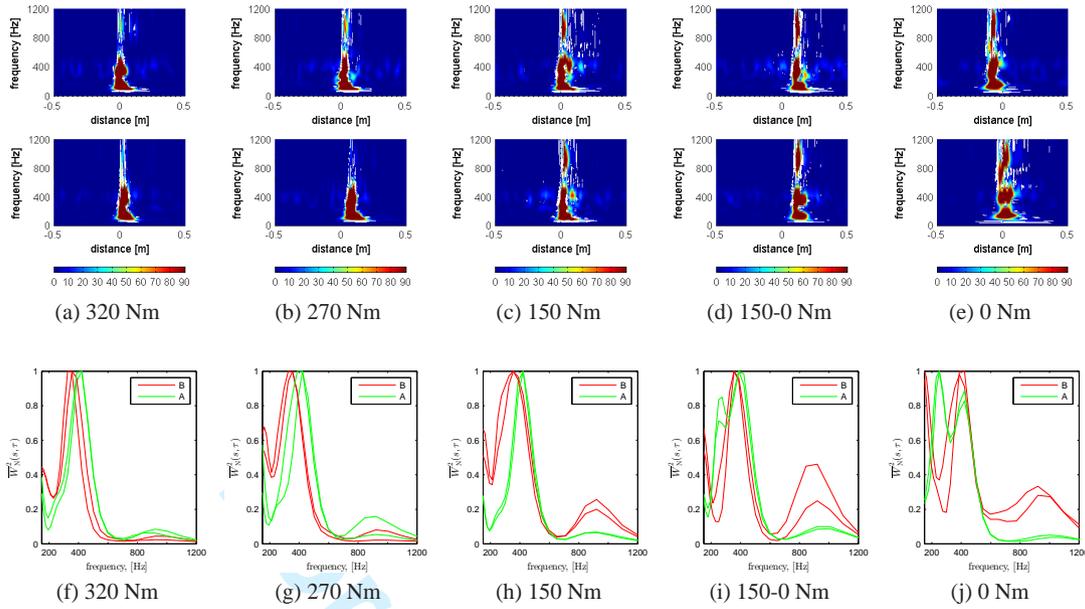
Figure 8. Scalograms for different bolt tightness conditions in B direction (a-e), and normalized global wavelet diagram for different bolt tightness conditions in A and B directions (f-j).

in Figure 9, the misalignment increases if the bolts become looser, so that the impact between wheel and rail is larger and consequently, the energy concentrated at this frequency increases. The increase in energy concentration at approximately 920 Hz is observed by comparing from left to right the normalized global wavelet spectrum diagrams in lower row in Figure 8).
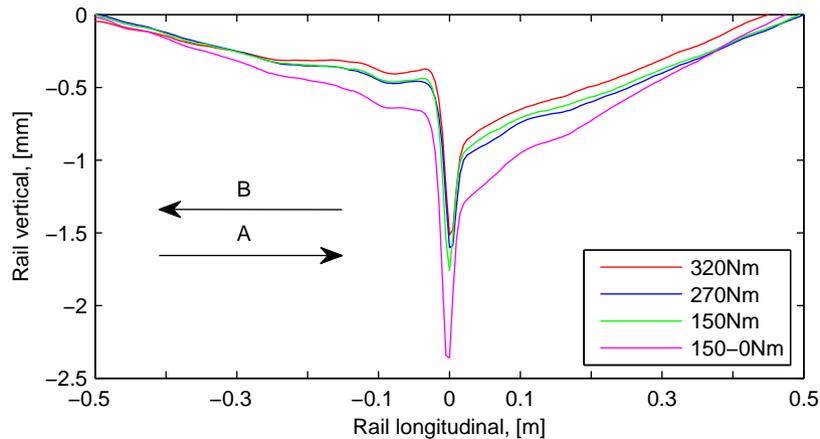

Figure 9. Measured rail vertical-longitudinal profile at the reference RJ for different bolt tightness conditions. Arrows indicate the rolling directions A and B.

In addition to the misalignment, the reassembling of the RJ may have altered other track components, such as the condition of the support in the vicinity of the reference RJ. The sleepers nearby the RJ may be slightly differently supported. Disturbances in sleeper and ballast conditions

may cause the difference in low frequency between the two running directions (i.e. peak at 150 or 250 Hz) because these track components are dominant contributors to the response of the track in this frequency range (24; 25).The differences in support conditions may also explain the two different slopes of the rail end tops towards the gap, as symmetry was expected because the traffic at the track site is bidirectional. These slopes may be caused by increased settlements, which are often larger at supports close to rail joints than at supports on continuous track due to higher loads (26). Plastic deformation of the rail end top may have also contributed to the development of the slopes. If the wheel-rail contact forces due to impact are high enough, plastic deformation occurs on the rail top after the gap. Consequently, the hardness of the rail top increases, as it was measured at insulated rail joints (27). The field observations of (27) showed that the hardness decreases with distance with respect to the gap. This is, less plastic deformation occurs further from the gap, and consequently, an slope develops on the rail top. In our case, as the track studied is bidirectional, the plastic deformation may have happened on both rail end tops resulting in two slopes. Also, slight different rolling conditions may have led to differential wear. In summary, the slope of the rail ends towards the gap may be caused by increased settlements and plastic deformation.

3.4. Bolt Tightness and Alignment Detection Algorithm

A detection algorithm is proposed based on the analysis of the measurements at the reference RJ. The decisions are taken according to the value of the normalized global wavelet spectrum $\overline{W}_{\mathrm{N}}^2(s,\tau)$ from (4) at the identified three characteristic frequencies: (1) 250 Hz (A direction) or 150 Hz (B direction), (2) 380-420 Hz and (3) 920 Hz. The parameters of the algorithm are tuned according to the experimental analysis described in the previous section. The detection algorithm evaluates bolt tightness condition of half RJ after the discontinuity, which is the half RJ excited by the wheel-rail impact. So for instance, bolts number 1 and 2 can be assessed when the tram travels in A direction; whereas bolts number 3 and 4 when the tram travels in B direction. The following simple expert system with three steps is proposed:

Step 1 Is the half RJ tight?

- A direction:
  - If $\overline{W}_{\mathrm{N}}^2(s,\tau)$ at 250 Hz is ≥ 0.6, then the half RJ is *loose* or *half-tight*.
  - Otherwise, if $\overline{W}_{\mathrm{N}}^2(s,\tau)$ at 250 Hz is < 0.6, then the half RJ is *tight*.
- B direction:
  - If $\overline{W}_{\mathrm{N}}^2(s,\tau)$ at 150 Hz is ≥ 0.6, then the half RJ is *loose* or *half-tight*.

– Otherwise, if $\overline{W}_N^2(s,\tau)$ at 150 Hz is < 0.6, then the half RJ is *tight*.

Step 2 If the half RJ is not tight,

- A or B direction:

    – If $\overline{W}_N^2(s,\tau)$ around 380-420 Hz is ≈ 1, then the half RJ is *half-tight*.

    – Otherwise, if $\overline{W}_N^2(s,\tau)$ around 380-420 Hz is < 1, then the half RJ is *loose*.

Step 3 Is there a misalignment between rail ends?

- A or B direction:

    – If $\overline{W}_N^2(s,\tau)$ around 920 Hz is ≥ 0.1, then there is misalignment.

    – Otherwise, if $\overline{W}_N^2(s,\tau)$ around 920 Hz is < 0.1, then there is not misalignment.

4. CASE STUDY

The proposed methodology to monitor bolt tightness condition was assessed by investigating two rail joints that were not used for tuning the detection algorithm. First the detection algorithm predicted their condition based on measured ABA signals, and later the bolt tightness condition was measured on the field. In this manner, the prediction was verified.

4.1. Track site

The test track site was the Meadow hall curve of the Supertram network in Sheffield. An overview of the test location is shown in Figure 10a. The traffic runs in both directions. The BS-80A rail, with 1/40 inclination, was supported by wooden sleepers every 0.6 m. There were no railpads in the track. At rail joints, the nominal rail gap was 6 mm. The two rail joints chosen for validation (hereinafter denoted as RJ3 and RJ5) are on the outer rail and are shown in Figure 11a and 11e. The locations of the two rail joints with respect to the reference RJ is shown in Figure 10b.

4.2. Prediction

The axle box responses to RJ3 and RJ5 were measured during the tests. The measured ABA signals were post-processed, and the scalograms and normalized global wavelet spectra calculated as shown in Figure 11. For the two rail joints of validation, the RJ characteristic frequency is observed at 420 Hz in both travel directions, in contrast to the reference RJ which showed two different characteristic frequencies at 380 and 420 Hz depending on the rolling direction (see Figure 8). Whereas RJ3 and
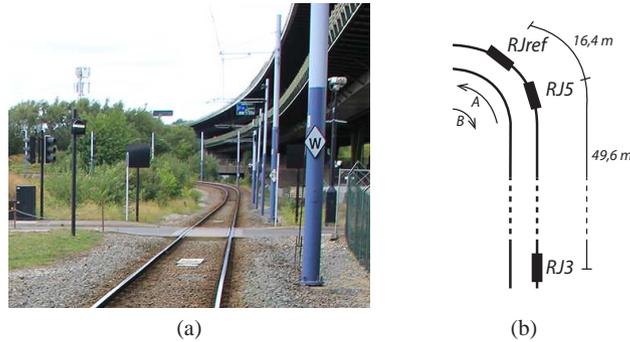
14   M. OREGUI ET AL.

(a)   (b)

Figure 10. (a) Test track site, (b) location of the RJs

(a)   (b)   (c)   (d)

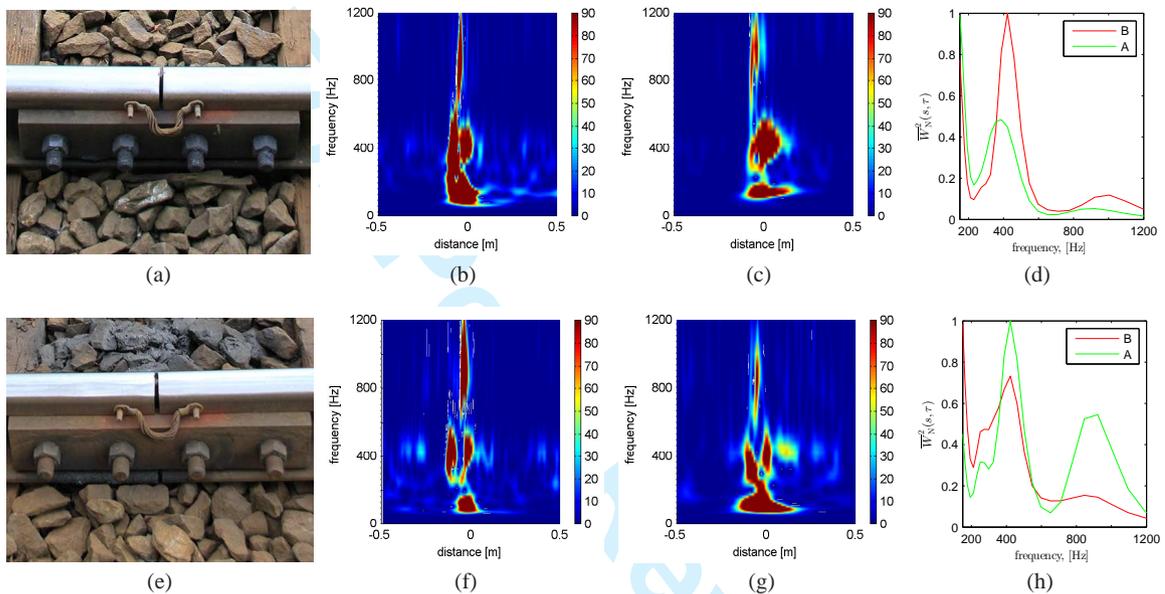(e)   (f)   (g)   (h)

Figure 11. For RJ3: (a) photo of RJ3, (b) scalogram in A direction for RJ3, (c) scalogram in B direction for RJ3, (d) normalized global wavelet spectrum diagram in A and B directions. For RJ5: (e) photo of RJ5, (f) scalogram in A direction for RJ5, (g) scalogram in B direction for RJ5, (h) normalized global wavelet spectrum diagram in A and B directions.

RJ5 were in the track for a long time before the time of the measurements, the condition of the reference RJ was changed one week before the measurements. This altered the supports nearby the reference RJ so that there is a difference in characteristic frequency between the two running directions. In time, a convergence on 420 Hz is expected for the reference RJ.

Once the measured data is post-processed, the predictions of bolt tightness conditions were made employing the detection algorithm of Section 3.4. For RJ3, the first half of the RJ was predicted as *half-tight* and the second half of the RJ was predicted as *loose*. For RJ5, the first half of the RJ was predicted as *loose*, whereas the other half of the RJ was predicted as *tight*. The prediction is graphically shown in Figure 12a. Regarding misalignment between rail ends, misalignment is predicted in RJ5, unlike RJ3 where the rail ends are predicted to be aligned.
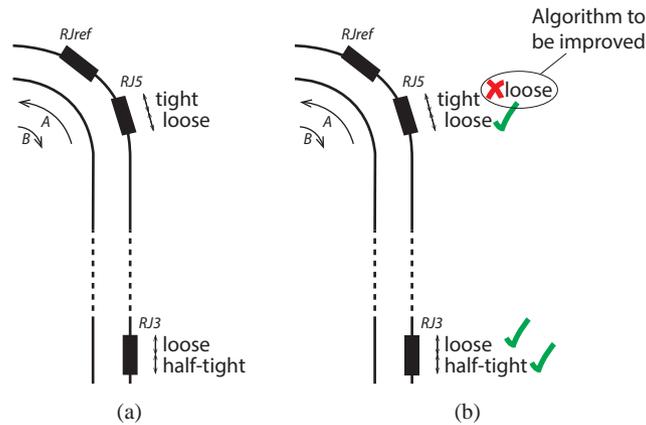
Figure 12. (a) Prediction and (b) Verification

4.3. Verification

The prediction of the tightness conditions of RJ3 and RJ5 was made in Delft, while it was checked by the 5th author at Supertram on 23 September 2011 (one month after the ABA measurements). Between the ABA measurements and the verification, no maintenance measures were taken on the test site so that no significant change was expected for the RJs. The tightness of each bolt was checked using a torque of 100 Nm, 200 Nm and 270 Nm. In the first step, the four bolts of the two RJs used for validation tolerated the torque of 100 Nm. In the second step, for RJ5 all four bolts showed a torque smaller than 200 Nm, thus the four bolts are *loose*. Regarding RJ3, the bolt tightness condition was different between the two RJ halves. The bolts at the first half of RJ3 in the A direction tolerated a torque of 200 Nm, not being able to reach the nominal value of 270 Nm, thus their condition was considered *half-tight*. In the second half, the bolts did not tolerated a torque of 200 Nm, thus the two bolts are *loose*.

The comparison between the prediction and verification is graphically shown in Figure 12b. The prediction for RJ3 and RJ5 agree with the verification for overall looseness condition of the rail joints. For each half of rail joints, the tightness prediction was correct for RJ3, but only for half of RJ5. Concerning misalignment between rail ends, no rail vertical-longitudinal profiles were measured at RJ3 and RJ5 for verification.

5. DISCUSSION: APPLICATION RANGE OF ABA SYSTEMS

ABA systems are under development, the analysis and diagnosis tools are improving. Those developments require a proper experiment design, so that under controlled conditions characteristics

of the track can be correctly correlated with ABA measurements. In this paper, a method to monitor invisible damage, such as loose bolts, was presented using an ABA system. In addition to the ability to detect invisible damage, the experimental analysis has given insight into the capacity of ABA systems regarding measurement speed and vehicle type.

First, measurements were performed at 21 km/h, which is significantly lower than the usual ABA measurement speeds of 80-100 km/h (18). High speeds are commonly employed because wheel-rail impact is larger at small defects such as light squat, so that signature tunes are excited with more energy, and consequently, they are easier to find in measured signals. At rail joints, the opposite happens. Contrary to small rail defects, the discontinuity between rail ends is large (i.e. 6 mm gap) so that when the wheel rolls over the discontinuity large impact occurs, even at low rolling speeds. Thus, although high rolling speeds are employed to shorten measurement times, ABA systems are able to detect defects at low speeds.

Second, the ABA prototype system was installed in a tram. The vehicle was significantly lighter than the vehicles usually employed in mainlines. The vehicle weight could have affected the analysis because lighter vehicles cause smaller impacts than heavier vehicles and consequently, signature tunes are excited with less energy which may make the detection more difficult. However, the ABA detection system worked when mounted in the tram.

Third, the presence of flexible wheels (also called resilient wheels) did not hinder the detection capacity of the ABA measurement system. Resilient wheels are used to prevent some of the track vibrations from reaching the vehicle and to reduce acoustic noise levels. In the case of this paper, the resilient material layer between wheel tyre and web did not eliminate the signature tunes related to bolt tightness and rail end misalignment. The influence of resilient wheels on detecting other type of defects should be investigated in the future.

In summary, the successful experimental investigation has shown that ABA systems could be employed in light rail systems, such as tram and metro lines, where rolling speeds are usually lower than in mainlines, vehicles are lighter and resilient wheels are often used.

6. CONCLUSIONS

The capacity of Axle Box Acceleration (ABA) detection and monitoring system for evaluating bolt tightness condition at rail joints (RJs) was experimentally investigated. First, the detection algorithm was developed based on controlled tests at a RJ with different bolt tightness conditions. Then, the bolt tightness condition of other RJs was used for verification of the method.

The experimental analysis has shown that:

- From ABA measurements, three states can be distinguished: tight RJ, intermediate loose RJ and completely loose RJ.
- ABA detection systems may be used for light rail systems, low speeds and resilient wheels.

Future work include the further extension of the ABA detection system to other types of damage at rail joints, such as cracks in the rail web, insulated rail joints, which are found in many networks worldwide, and broad range of speed, from metros to conventional railways. Developing numerical models is also part of future work so that, for example, the vibration modes related to the characteristic frequencies can be identified. Although measurements are required for calibration and validation, the ABA system extension can be faster and easier based on more flexible and relatively fast numerical models than on time-consuming, expensive and safety threatening field testing.

APPENDIX A. NUMERICAL MODAL ANALYSIS OF THE RESILIENT WHEEL

ABA measurements include both wheel and track vibrations. Thus, wheel vibrations should be differentiated from track vibrations when ABA measurements are analyzed. One way to obtain information of wheel dynamics is by modal analysis. For this purpose, a free suspended finite element (FE) of the test resilient wheel is developed. Figure 13a and 13b show the single resilient wheel and the half of the axle considered. The longitudinal direction is denoted as x, the lateral as y, the vertical as z. The wheel consists of steel and has 22 rubber blocks between the tyre and the web. A simplified nominal cross-section of the wheel is used and the rubber is modeled as a straight band covering the whole width of the wheel to facilitate the modeling. The lateral confinement of the rubber is considered by coupling in the y-direction the displacements of the nodes on the lateral surfaces of the rubber.

In modal analysis, materials are linear. Thus, the resilient wheel's steel and rubber are defined as elastic. For the steel, the Young's modulus is 210 GPa, Poisson's ratio is 0.3 and density is 7800 kg/m^3. Regarding the rubber, its properties significantly influence the dynamic behavior of the wheel (28). The density is 1190 kg/m^3 and the Poisson's ratio is assumed to be 0.49. The Young modulus is obtained from laboratory force-displacement compression tests in which the molds of the test resemble the real v-shape web-rubber-tyre geometry, see Figure 14a. The resulting force-displacement curve is shown in Figure 14b. The rubber is pre-stressed when mounted in the wheel
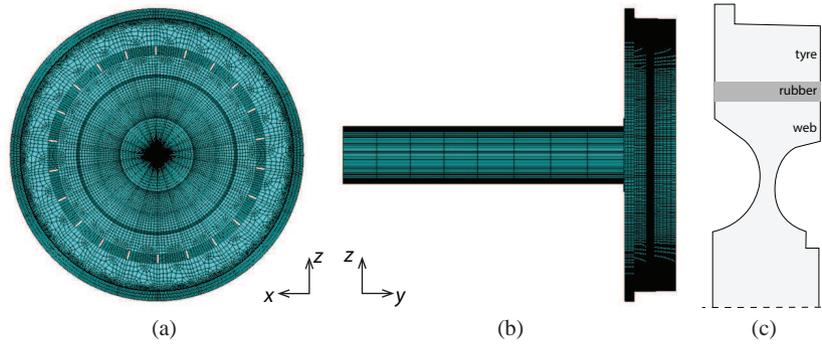
Figure 13. Finite element model of the resilient wheel and axle (a) front view, (b) side view, and (c) cross-section of the wheel.

so that the working condition is defined between 8.3 and 9.3 mm. In this range, the Young's modulus is 75 MPa.
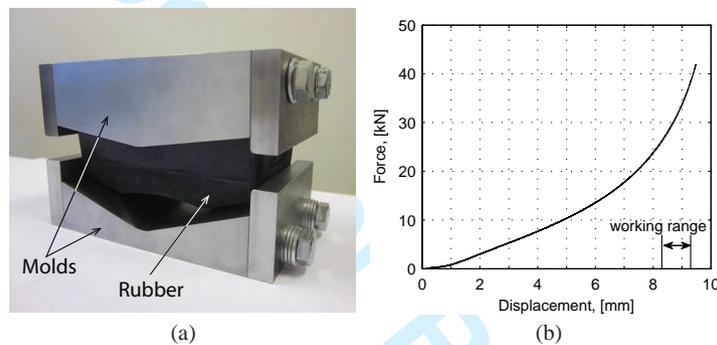

Figure 14. (a) Rubber and testing molds assembly (b) Measured force-displacement curve.

The resilient wheel modes between 50 and 1200 Hz are shown in Figure 15, where the colors indicate the amplitudes of the vibrations. The modes are axle modes or wheel modes and within the wheel modes, they can be web modes or tyre modes (29). In the web modes, the web vibrates while the tyre barely moves due to the decoupling introduced by the rubber. In the tyre modes, the opposite happens. Further, the web and tyre modes can be classified as axial (i.e. out-of-plane deformation), radial (i.e. in-plane radial deformation) and tangential (i.e. in-plane tangential deformation) (29), where the in-plane is the *xz* plane, see Figure 13.

These vibration modes can be used in the ABA measurements study because the free suspended wheel approach replicates almost all the wheel vibration modes obtained with the laid down wheel (30; 31; 32). The difference is that extra two(or more)-nodal-diameter axial modes appear due to the imperfect axial-symmetry of the wheel in contact with the rail (33; 30). For the resilient wheel investigated in the frequency range of 50-1200 Hz, two axial tyre modes would result into more modes when the wheel is supported. At RJs, however, the wheel modes excited will mostly be

in-plane deformations (i.e. radial and tangential modes) because the impact at RJs is in the vertical (xz) plane. Furthermore, the tyre modes will be measured significantly attenuated at the vertical (z) accelerometers located on the axle because of the uncoupling between the tyre and the web.
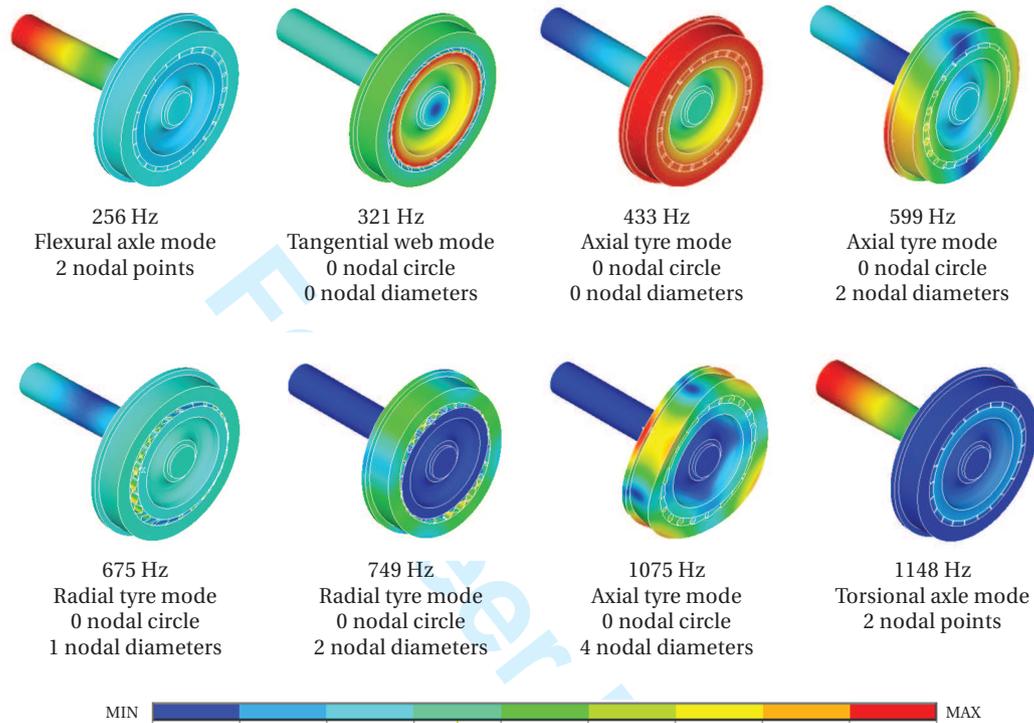

256 Hz	321 Hz	433 Hz	599 Hz
Flexural axle mode	Tangential web mode	Axial tyre mode	Axial tyre mode
2 nodal points	0 nodal circle	0 nodal circle	0 nodal circle
	0 nodal diameters	0 nodal diameters	2 nodal diameters

675 Hz	749 Hz	1075 Hz	1148 Hz
Radial tyre mode	Radial tyre mode	Axial tyre mode	Torsional axle mode
0 nodal circle	0 nodal circle	0 nodal circle	2 nodal points
1 nodal diameters	2 nodal diameters	4 nodal diameters	

MIN ▬▬▬▬▬▬▬▬▬▬ MAX

Figure 15. Resilient wheel mode shapes; the color shows displacement.

ACKNOWLEDGMENTS

REFERENCES

[1] Pang T, Dhanasekar M. Dynamic finite element analysis of the wheel-rail interaction adjacent to the insulated rail joints. *7th International Conference on Contact Mechanics and Wear of Wheel/rail Systems*, Brisbane, Australia, 2007.

M. OREGUI ET AL.

[2] Jenkins H, Stephenson J, Clayton G, Morland G, Lyon D. Effect of track and vehicle parameters on wheel/rail vertical dynamic forces. *Railw Eng J* 1974; **3**(1):2–16.

[3] Kabo E, Nielsen J, Ekberg A. Prediction of dynamic train-track interaction and subsequent material deterioration in the presence of insulated rail joints. *Vehicle System Dynamics* 2006; **44**(SUPPL. 1):718–729.

[4] Remennikov A, Kaewunruen S. A review of loading conditions for railway track structures due to train and track vertical interaction. *Structural Control and Health Monitoring* 2008; **15**(2):207–234.

[5] Li Z, Zhao X, Dollevoet R, Molodova M. Differential wear and plastic deformation as causes of squat at track local stiffness change combined with other track short defects. *Vehicle System Dynamics* 2008; **46**(SUPPL.1):237–246.

[6] Bandula-Heva T, Dhanasekar M, Boyd P. Experimental investigation of wheel/rail rolling contact at railhead edge. *Experimental Mechanics* 2013; **53**(6):943–957.

[7] Ph Papaelias M, Roberts C, Davis CL. A review on non-destructive evaluation of rails: State-of-the-art and future development. *Proceedings of the Institution of Mechanical Engineers, Part F: Journal of Rail and Rapid Transit* 2008; **222**(4):367–384.

[8] Mazzeo P, Nitti M, Stella E, Distante A. Visual recognition of fastening bolts for railroad maintenance. *Pattern Recognition Letters* 2004; **25**(6):669–677.

[9] Clark R. Rail flaw detection: Overview and needs for future developments. *NDT and E International* 2004; **37**(2):111–118.

[10] Loveday P. Guided wave inspection and monitoring of railway track. *Journal of Nondestructive Evaluation* 2012; **31**(4):303–309. Cited By (since 1996)4.

[11] Deliverable D21 of ACEM-Rail. Report on railway inspection and monitoring techniques analysis of different approaches. http://www.acem-rail.eu/documents.html 2011.

[12] Weston P, Ling C, Goodman C, Roberts C, Li P, Goodall R. Monitoring lateral track irregularity from in-service railway vehicles. *Proceedings of the Institution of Mechanical Engineers, Part F: Journal of Rail and Rapid Transit* 2007; **221**(1):89–100.

[13] Bocciolone M, Caprioli A, Cigada A, Collina A. A measurement system for quick rail inspection and effective track maintenance strategy. *Mechanical Systems and Signal Processing* 2007; **21**(3):1242–1254.

[14] Lee J, Choi S, Kim SS, Park C, Kim Y. A mixed filtering approach for track condition monitoring using accelerometers on the axle box and bogie. *IEEE Transactions on Instrumentation and Measurement* 2012; **61**(3):749–758.

[15] Molodova M, Li Z, Dollevoet R. Axle box acceleration: Measurement and simulation for detection of short track defects. *Wear* 2011; **271**(1-2):349–356.

[16] Cantero D, Basu B. Railway infrastructure damage detection using wavelet transformed acceleration response of traversing vehicle. *Structural Control and Health Monitoring* 2014; doi:10.1002/stc.1660.

[17] Oregui M, Li Z, Dollevoet R. Identification of characteristic frequencies of damaged railway tracks using field hammer test measurements. *Mechanical Systems and Signal Processing* 2014; **54**:224–242.

[18] Molodova M, Li Z, Núñez A, Dollevoet R. Automatic detection of squats in railway infrastructure. *IEEE Transactions on Intelligent Transportation Systems* 2014; **15**(5):1980–1990.

[19] Esveld, C. Railprof measurement device. http://www.esveld.com/railprof.htm 2014.

[20] Mandal N. Ratchetting of railhead material of insulated rail joints (irjs) with reference to endpost thickness. *Engineering Failure Analysis* 2014; **45**:347–362.

[21] Vetterli M, Kovacevic J. *Wavelets and Subband Coding*. Prentice Hall PTR, 1995.

[22] Torrence C, Compo G. A practical guide to wavelet analysis. *Bulletin of the American Meteorological Society* 1998; **79**(1):61–78.

[23] Percival D. On estimation of the wavelet variance. *Biometrika* 1995; **82**(3):619–631.

[24] Wu T, Thompson D. The effects of local preload on the foundation stiffness and vertical vibration of railway track. *Journal of Sound and Vibration* 1999; **219**(5):881–904.

[25] Sadeghi J. Field investigation on vibration behavior of railway track systems. *International Journal of Civil Engineering* 2010; **8**(3):232–241.

[26] Zong N, Askarinejad H, Heva T, Dhanasekar M. Service condition of railroad corridors around the insulated rail joints. *Journal of Transportation Engineering* 2013; **139**(6):643–650.

[27] Oregui M, Molodova M, Núñez A, Dollevoet R, Li Z. Experimental investigation into the condition of insulated rail joints by impact excitation. *Experimental Mechanics* 2015; **55**(9):1597–1612.

[28] Cigada A, Manzoni S, Vanali M. Geometry effects on the vibro-acoustic behavior of railway resilient wheels. *JVC/Journal of Vibration and Control* 2011; **17**(12):1761–1778.

[29] Periard FJ. Wheel-rail noise generation: curve squealing by trams. Phd, Delft University of Technology 1998.

[30] Cigada A, Manzoni S, Vanali M. On the vibro-acoustic behaviour of high-speed train wheels. 2006; 4283–4297.

[31] Cigada A, Manzoni S, Vanali M. Vibro-acoustic characterization of railway wheels. *Applied Acoustics* 2008; **69**(6):530–545.

[32] Glocker C, Cataldi-Spinola E, Leine R. Curve squealing of trains: Measurement, modelling and simulation. *Journal of Sound and Vibration* 2009; **324**(1-2):365–386.

[33] Thompson D. Wheel-rail noise generation, part iv: Contact zone and results. *Journal of Sound and Vibration* 1993; **161**(3):447–466.